An Experimental Study of the Trust Vector Control Using Counterflow Concept

C. M. Lim, H. D. Kim†, K. H. Lee and T. Setoguchi‡*

388, Songcheon, Andong, School of Mechanical Engineering, Andong National University, 760-749, Korea
1, Honjo, Department of Mechanical Engineering, Saga University, Saga 840-8502, Japan

kimhd@andong.ac.kr

Keywords: Coanda Effect, Compressible Flow, Counterflow Concept, Shock Wave, Thrust Vector Control

Abstract

Recently, fluidic thrust vectoring methods have been preferably employed to control the movement of propulsive systems due to relatively simpler design and lower cost than mechanical thrust vectoring methods. For An application of the thrust vectoring to flight bodies, it is necessary to understand very complicated exhaust flows which are often subject to shock waves and boundary layer separation. But researches for the thrust vector control using counterflow have been few.

In the present study, experiments have been performed to investigate the characteristics of supersonic jets controlled by a thrust vectoring method using counterflow. The primary jet is expanded through a two-dimensional primary nozzle shrouded by collars, and is deflected by the suction of the air near nozzle into an upper slot placed between the primary nozzle and the upper collar. A shadowgraph method is used to visualize the supersonic jet flowfields. Primary nozzle pressure ratios and suction nozzle pressure ratios are varied from 3.0 to 5.0, and from 0.2 to 1.0 respectively. The present experimental results showed that, for a given primary nozzle pressure ratio, a decrease in the suction nozzle pressure ratio produced an increased thrust vector angle. As the suction nozzle pressure ratios were increased and decreased, the hysteresis of the thrust vectoring was observed through the wall pressure distributions

Introduction

In general, it is important for the thrust vector control technique of propulsive rockets or aircrafts to aircraft system performance. Thrust vector control of propulsive jet not only increases the movement of the aircraft but also reduces the additional installation such as empennage increasing the aerodynamic drag.

Recently, a number of researches have been conducted to apply mechanical thrust vectoring methods using various equipments such as vanes installed in a nozzle and movable nozzles to the aircraft.[1-3] The method using jet vanes in the nozzle produces a large loss of stagnation pressure due to a shock wave system and a thermal load of the vanes. To use the movable nozzle requires additional power installation, increasing the weight, cost, and high-observability of aircraft.

Researchers are interested in the Fluidic thrust vector control, instead of the mechanical thrust vector control having these demerits. For the fluidic thrust vector control using the secondary injection flow[4-5], the problems related to the complex mixture of two flows and the optimum design are not fully understood yet nozzle using the secondary injection flow.

Lately, counterflow method involving fluidic thrust vectoring is of great interest.[6-8] These generally use the thrust vectoring occurred by creating counterflowing a secondary air stream with the application of suction at a slot between the primary nozzle and an aft collar.

To a practical application of the thrust vectoring using counterflow method to flight bodies, it is necessary to understand very complicated exhaust flow which is often subject to shock waves, Coanda effect, and boundary layer separation. But researches for the thrust vector control using counterflow have been few.

In the present work, experiments were performed to investigate the characteristics of supersonic jets controlled by a thrust vectoring method using counterflow. The geometric variables investigated include collar geometry. The nozzles are tested at static conditions. The effects of the suction rate and Coanda surface geometry on the forces generated have been investigated by measuring the static pressure distributions along nozzle walls. A shadowgraph method was used to visualize jets expanded from the primary nozzle and deflected by the suction.

Facilities

Fig.1 shows experimental apparatuses used in the present study. The majority of measurements was conducted in the blow-down compressed air wind tunnel. High pressure air of a primary tank is supplied air compressor. Vacuum pump inhales the air from a suction tank. High pressure air which passes a primary nozzle of design Mach number 1.5 is supersonic jet and then discharges into the atmosphere. The inhalation from a suction tank of low pressure is supplied to the upper slot between the primary nozzle exit and the upper suction collar. The lower slot is connected to the atmosphere. Primary nozzle pressure ratio(NPR_p) and suction nozzle pressure ratio(NPR_s)

* Dep. of Mech. Eng., Andong National University
† School of Mech. Eng., Andong National University
‡ Dep. of Mechanical Engineering, Saga Univ.

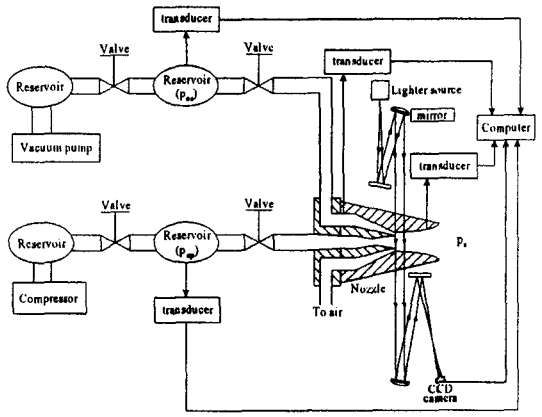

Fig. 1 Experimental apparatus

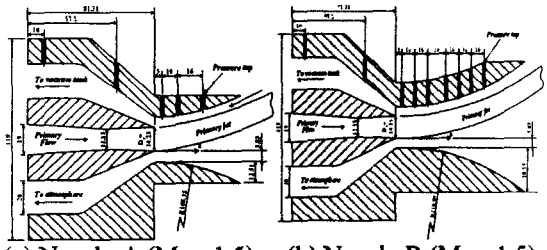

(a) Nozzle-A (M_a = 1.5) (b) Nozzle-B (M_a = 1.5)

Fig. 2 Nozzle Configurations

are varied from 3.0 to 5.0, and from 0.2 to 1.0 respectively. A shadowgraph method using the Xe lighter source is used to visualize jets expanded from primary nozzle and deflected by the suction. The static pressure is measured by the pressure sensor connected to the transducer and is kept by the personal computer.

Fig.2 shows the schematic diagrams of nozzle used in the experiment. The primary jet is expanded through two-dimensional primary nozzle shrouded by collars, and is deflected by the suction of the air near nozzle into the upper slot between the primary nozzle and the upper collar. The static pressures along the upper suction collar are measured by the pressure sensors installed at the pressure tabs. The diameter of the primary nozzle exit defines as D_e and the distance from the primary nozzle exit through the primary jet defines as x. The radius of curvature of suction collars is 108.35mm and 216.69mm, respectively.

Results and Discussions

Fig.3 shows the shadowgraph photographs. As NPR_s decreases, the primary jet is deflected by the Coanda effect. Consequently, the primary jet is attached to the upper suction collar and an attached point of jet is moved to upstream. At NPR_s = 0.3, the normal shock wave is at the downstream of an attached jet

Fig.4 shows the static pressure distributions along suction collar for the Nozzle-A. The horizontal axis shows the non-dimensional x/D_e which is a ratio of the distance from primary nozzle exit, x, to the diameter of the primary nozzle exit, D_e. The vertical axis shows

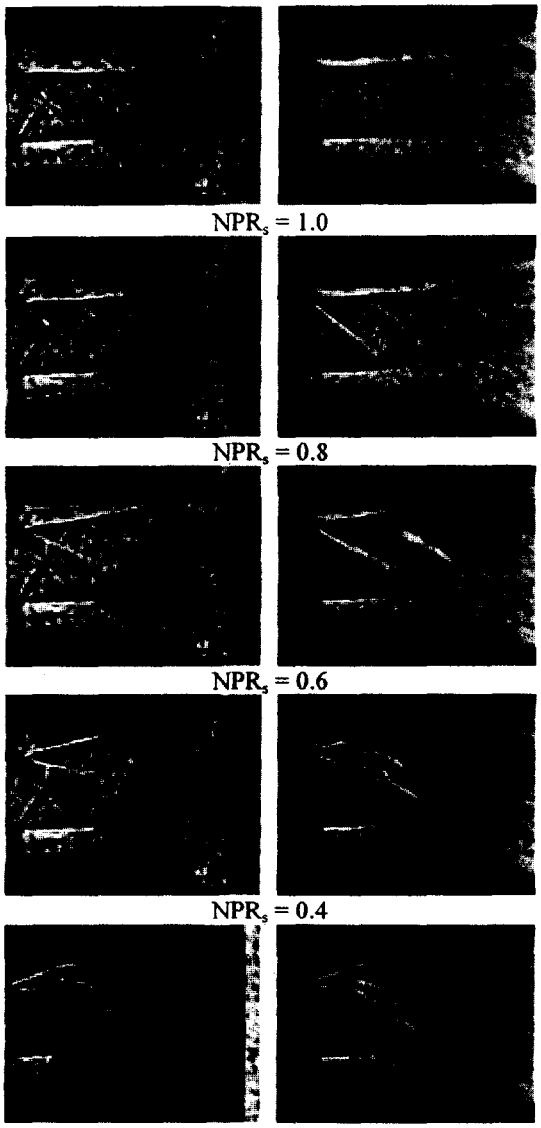

(a) Nozzle-A (M_a = 1.5) (b) Nozzle-B (M_a = 1.5)

Fig. 3 Shadowgraph Photographs (NPR_p = 3.6)

the non-dimensional p_w/p_a which is a ratio of the static pressure along suction collar, p_w, to the atmosphere, p_a. For $x/D_e < 0.4$ of Fig.4 and 5, the static pressure distribution gives rise to the subatmosphere because of the mass inhaled by applying suction to the upper slot and the mass discharged due to a reaction between the primary jet and the surrounding near the nozzle exit. For Fig.4(b), at x/D_e=1.0526 and $NPR_s \leq 0.4$, the oblique shock wave generated in jet attached to the upper collar surface increases the static pressure along the upper suction collar. For Fig.4(c) at the same condition, the stronger oblique shock wave due to inclined collision of the under-expanded primary jet against the suction collar increases suddenly the static pressure along the upper suction collar.

Fig.5 shows the static pressure distributions along suction collar for the Nozzle-B. As NPR_s is decreased,

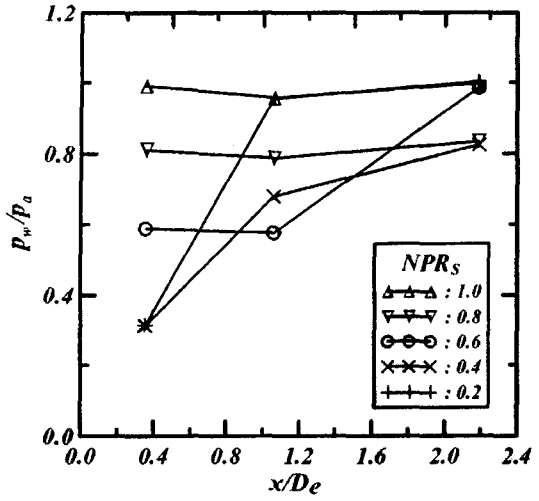

(a) NPR_p = 3.0

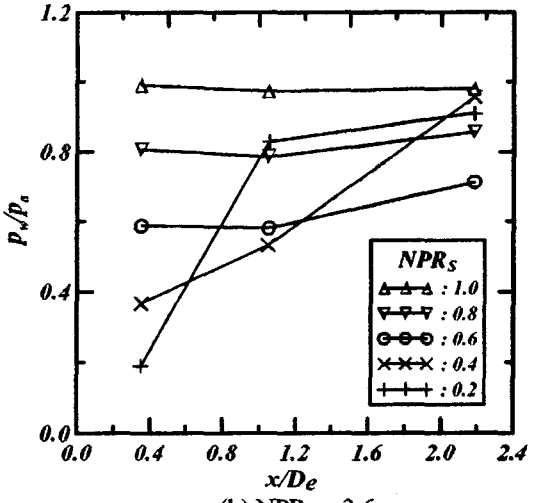

(b) NPR_p = 3.6

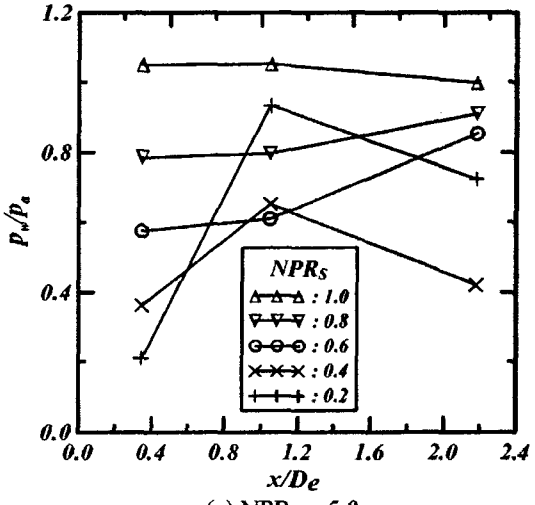

(c) NPR_p = 5.0

Fig. 4 Static pressure distributions along the upper suntion collar(Nozzle-A)

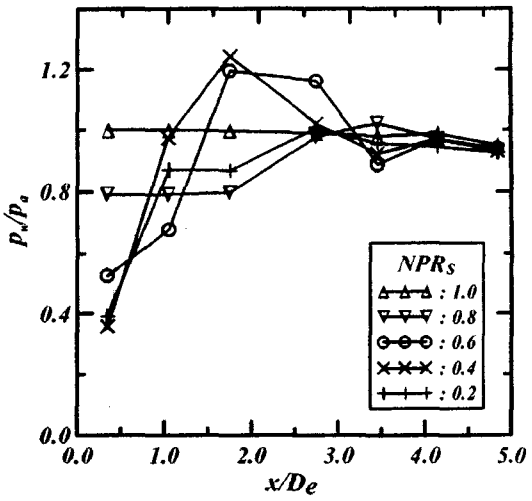

(a) NPR_p = 3.0

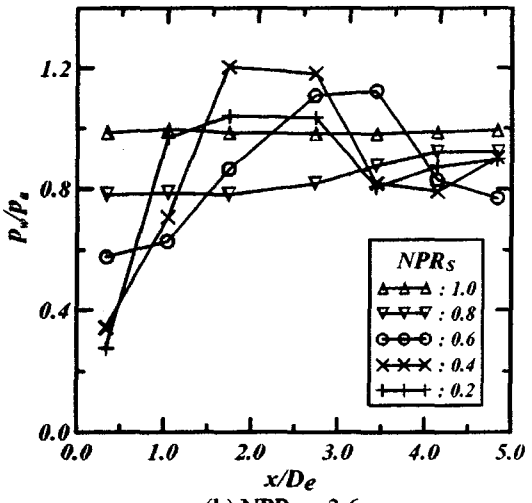

(b) NPR_p = 3.6

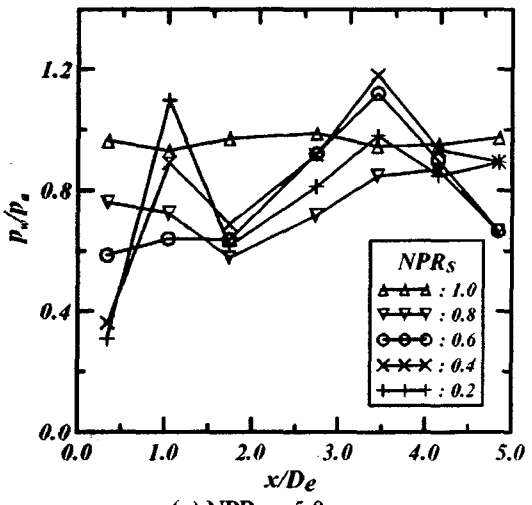

(c) NPR_p = 5.0

Fig. 5 Static pressure distributions along the upper suction collar(Nozzle-B)

p_w/p_a of the maximum is shift to the upstream. For Fig.5(a), 5(b), at NPR_s < 0.4 and x/D_e < 2.0, the oblique shock wave generated from a inclined collision of the jet against the upper collar surface

increases the static pressure distribution along the upper suction collar. For Fig.5(c) at NPR_s = 0.4, p_w/p_a is increased and decreased because of the direct collision of the jet and supersonic flow, and then maximum of p_w/p_a is about x/D_e=3.4386. The reason is the normal shock wave generated in jet attached. At NPR_s = 0.2, because the direct collision of the jet and the stronger oblique shock wave are generated to the upstream, the point of maximum p_w/p_a is the upstream than that of NPR_s = 0.2.

Fig.6 shows the relationship the NPR_s with the jet deflection angle(α) for a given NPR_p and nozzle configuration. α defines the angle of x axis and the center axis of primary jet, and L_a defines the distance from the primary nozzle exit to the point attached for the expanded jet to the suction collar. As NPR_p is increased and NPR_s is decreased, α is increased because of a NPRs of the suction slot and a under-expanded primary jet. For NPR_p=3.6 which is the design pressure ratio, α is minimum because this pressure ratio produces the maximum thrust. The others ratios, except NPR_p=3.6, are less the thrust than that of the NPR_p=3.6, but the thrust vectoring is effectively.

Fig.7 presents the relationship the NPR_s with the jet attachment length(L_a/D_e) for a given NPR_p and nozzle configuration. As NPR_p is increased and NPR_s is decreased, L_a/D_e is decreased. Because the lower NPRs at the upper suction slot produces the more expanded primary jet. Consequently, the attached point of the expanded jet boundary to the upper collar is shifted to upstream.

As the NPR_s is increased and decreased, Fig.8 and 9 present the hysterics characteristics. At Fig.8(a) and Fig.9(a), the locus of p_w/p_a distribution of increasing NPR_s is higher than decreasing NPR_s. At Fig.8(a) and Fig.9(a), the locus of p_w/p_a distribution is inverse. Fig. 9 also presents the similar tendency.

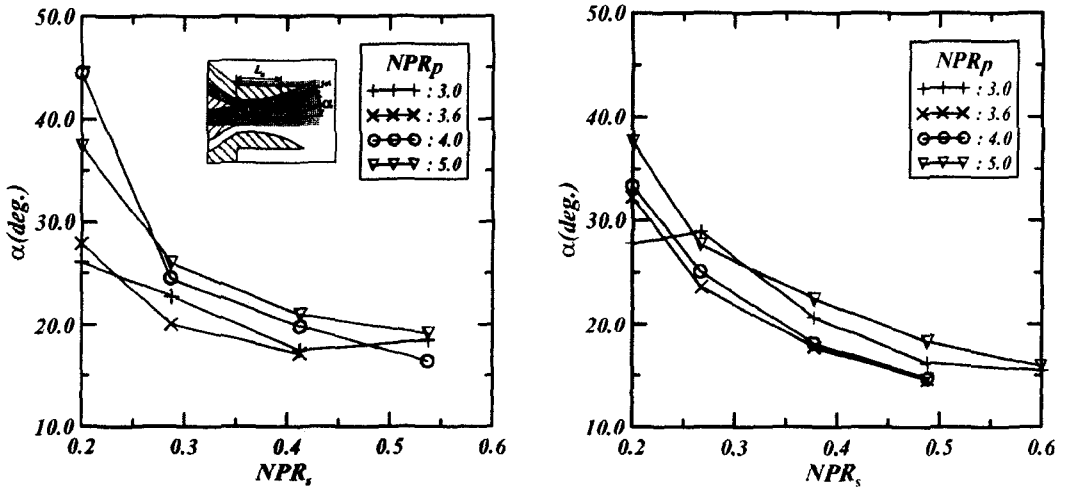

(a) Nozzle-A (b) Nozzle-B

Fig. 6 Jet deflection angle

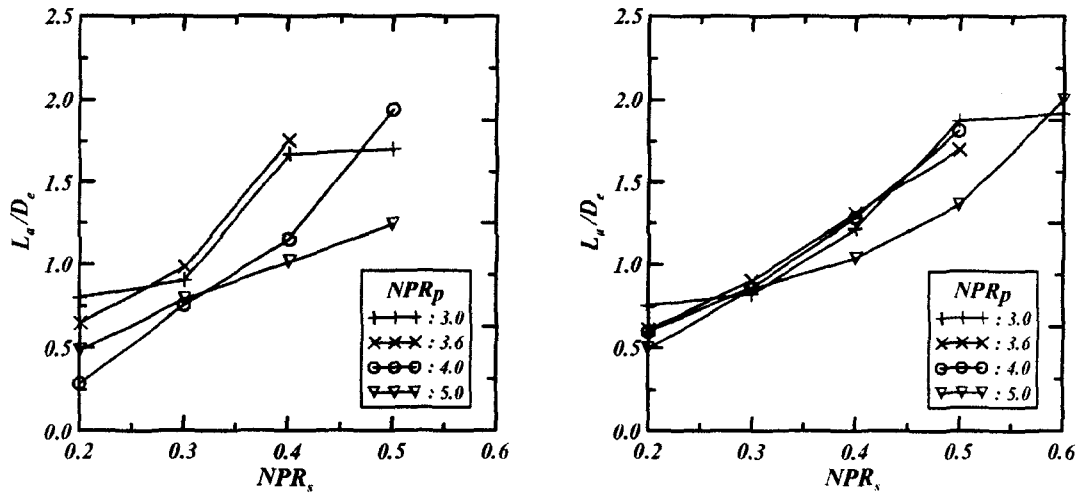

(a) Nozzle-A (b) Nozzle-B

Fig. 7 Jet attachment lengths

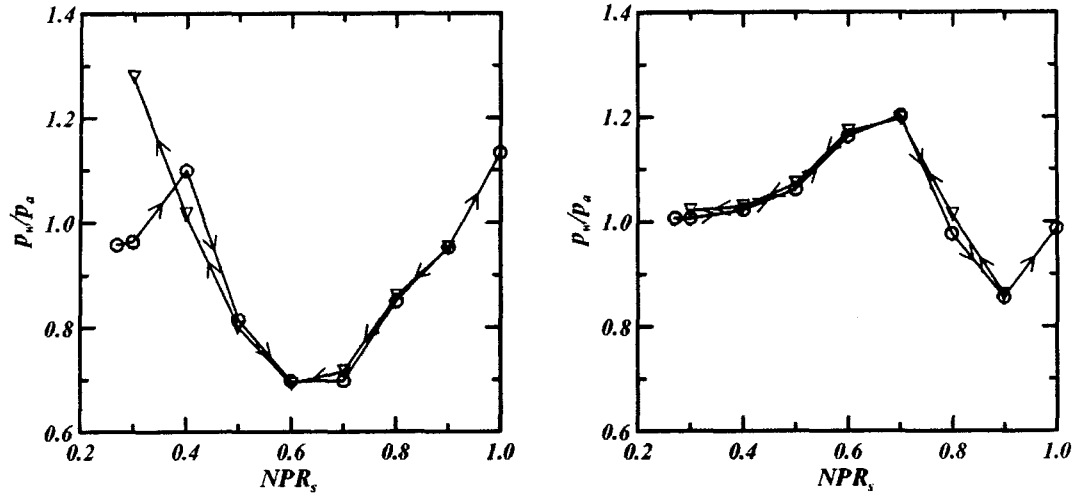

(a) $x/D_e = 1.05$ (b) $x/D_e = 2.74$

Fig. 8 Hysterics characteristics (Nozzle-B, $NPR_p = 3.0$)

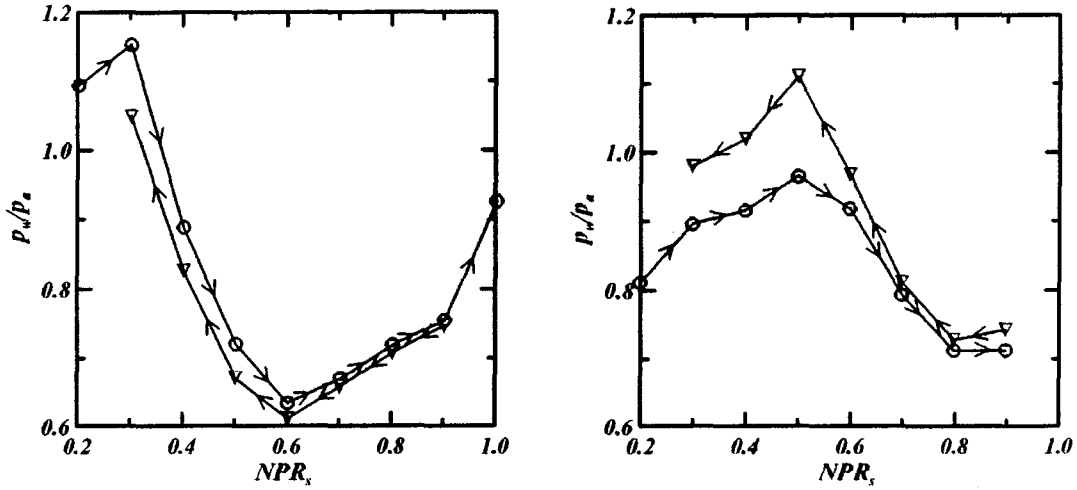

(a) $x/D_e = 1.05$ (b) $x/D_e = 2.74$

Fig. 9 Hysterics characteristics (Nozzle-B, $NPR_p = 5.0$)

Fig.8(a) and Fig.9(a) show that, for the increasing NPR_s, the attached point is shifted to downstream and the oblique shock wave in the attached jet increases the p_w/p_a. For Fig.8(a) at $0.4 < NPR_s < 0.6$ and Fig.9(a) at $0.3 < NPR_s < 0.6$, an expanded jet is detached from the suction collar. For Fig.8(a) and Fig.9(a) at $NPR_s > 0.6$, a detached jet leads to the mass entrainment from the surrounding and then static pressure on the suction collar is recovered as the atmosphere. A p_w/p_a distribution of case which decreases NPR_s is similar to the case increasing NPR_s. At $NPR_s < 0.5$ of Fig.8(a) and at $NPR_s < 0.9$ of Fig.9(a), the different locus of p_w/p_a for increasing NPR_s and decreasing NPR_s appears as the hysteresis phenomenon. Fig.8(b) shows that, for increasing NPR_s, a jet attachment point is moved to downstream and the oblique shock wave in the attached jet increases the p_w/p_a. At $0.7 < NPR_s < 0.9$ of Fig.8(b) and at $0.5 < NPR_s < 0.8$ of Fig.9(b), an expanded jet is detached from the suction collar. At $NPR_s > 0.9$ of Fig.8(b), a detached jet leads to the mass entrainment from the surrounding and then static pressure on the suction collar is recovered as the atmosphere. A p_w/p_a distribution of case which decreases NPR_s is similar to the case increasing NPR_s. For all NPR_s at two points, in general, the different locus of p_w/p_a distribution of increasing NPR_s and decreasing NPR_s appears as the hysteresis phenomenon.

Conclusion

In the present work, experiments were performed to investigate the characteristics of supersonic jets controlled by a thrust vectoring method using counterflow. The present experimental results showed that:

1) For a given NPR_p, a decrease in the NPR_s produced an increased thrust vector angle.

2) For the design pressure ratio, α is minimum because this pressure ratio produces the maximum thrust. The others ratios, except NPR_p=3.6, are less the thrust than that of the NPR_p=3.6, but the thrust vectoring is effective.
3) For higher NPR_p, the difference of the hysteresis phenomenon is remarkable.

References

1) Bitten R. and Selmon J.: Operational Benefits of Thrust Vector Control(TVC), *High-Angle-of-Attack Technology, vol.1, J.R. Chambers, W.P. Gilbert, And L.T. Nguyen, eds., NASA CP-3149, Part 2,* 1992.
2) Herbst W. B.: Future Fighter Technologies, *J. Aircraft, vol.17, No.8,* 1980.
3) Herrick P. W.: Propulsion Influences on Air Combat, *AIAA-85-1457,* 1985
4) Jung, S. J., Kim, H. D., Ahn, J. M. and Jung, D. H.: Study of the Thrust Vector Control Using a Secondary Flow Injection, *Proc. KSPE Spring Annual Meeting,* 2002, pp.14-15
5) Green, C. J. and McCullough, M. Jr.: Liquid Injection Thrust Vector Control, *AIAA J., vol.1, No.3,* 1963, pp.573-578
6) Flamm, J. D.: Experimental Study of a Nozzle Using Fluidic Counterflow Thrust Vectoring, *AIAA 98-3255,* 1998.
7) Hunter, C. and Wing, D.: Counterlow Thrust Vectoring: Control Volume Similarity Analysis, *NASA Langley Research Center White Paper,* 1995.
8) Hunter, C. A. and Deere, K. A.: Computational Investigation of Fluidic Counterflow Thrust Vectoring, *AIAA-99-2669,* 1999.